APPENDIX A: 3D SIMULATION WITH MINIMUM V_S OF 200 M/S

In this study, we constrained our 3D simulations to using $V_S > 500$ m/s due to limitations in computational resources, and added 1D corrections for the effects of the material with $V_S \leq 500$ m/s. In order to assess the effect of these 1D corrections we used a 3D simulation of the La Habra earthquake with CVM-S and a minimum V_S of 200 m/s obtained from a discontinuous mesh (DM) version of AWP (Nie *et al*., 2017). The simulated domain (Table 1) is discretized into three partitions: 1) dx=8 m from the surface to 1,472 m, 2) dx=24 m between 1,472 m and 10,336 m, and 3) dx=72 m at deeper levels. The improved efficiency of the DM approach allows us to lower the minimum V_S to 200 m/s and retain 5 points per minimum S-wavelength. The reason for not using the more efficient DM code for other simulations in this study is that the code is currently limited to a flat free surface condition.

Fig. A1 shows the FAS bias of two 3D simulations for Model 17 (see Table 2) with minimum V_S of 200 m/s and 500 m/s, both using a flat free surface boundary condition. Since the lower velocity material has very little effect on the vertical component, we apply the correction to the horizontal components only. The SH1D correction (with the minimum V_S clamped at 200 m/s) is applied to the horizontal components of the 3D simulation with minimum V_S of 500 m/s. For the horizontal components, the corrected simulation matches the minimum V_S of 200 m/s simulation fairly well, with less than 10% difference in terms of the median bias below about 2.5 Hz. The moderate overprediction for higher frequencies up to 5 Hz ($<$ about 25%) is likely caused by vertical resonance effects primarily in the 1D model.

SUPPLEMENTARY MATERIAL

Supplementary materials are available at *GJI* online.

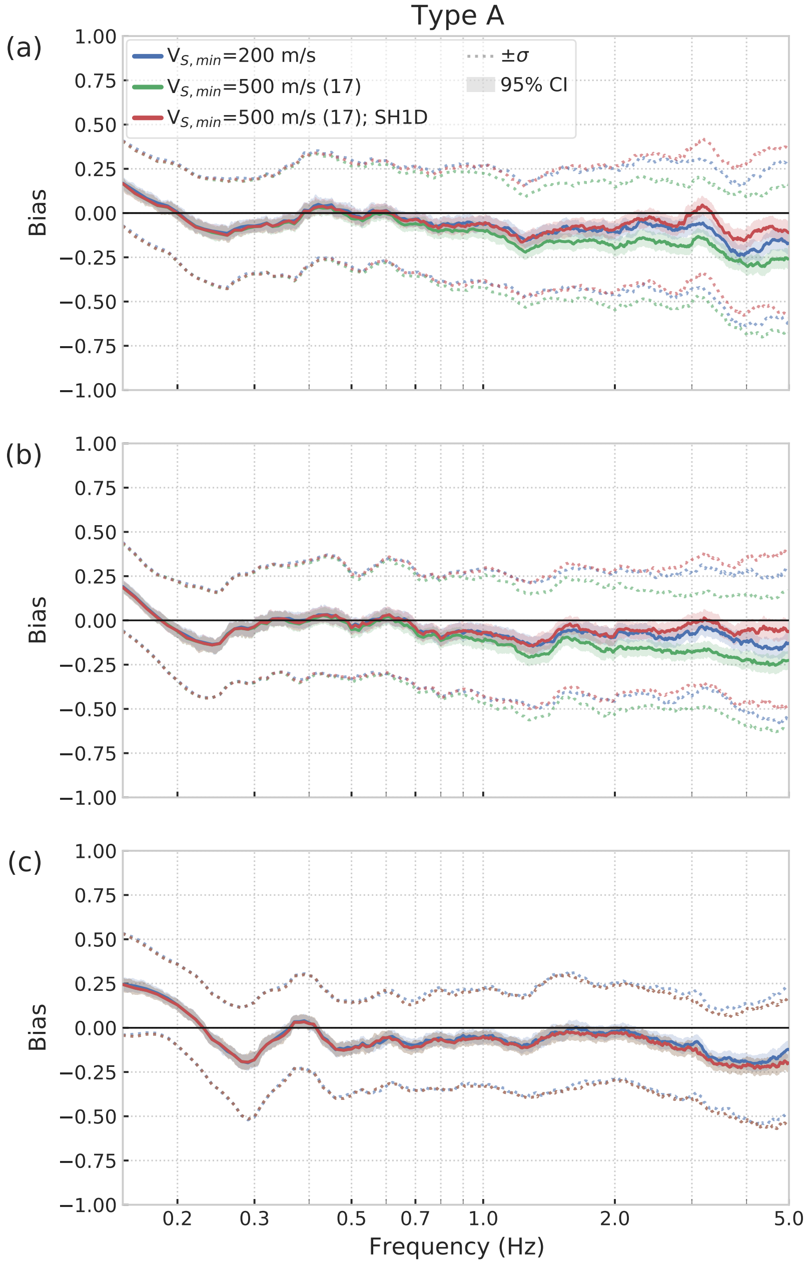

Figure A1: FAS bias between data and synthetics with minimum V_S clamped at 200 m/s (blue), 500 m/s (green), and 500 m/s with 1D correction (red) for (a) E-W, (b) N-S, and (c) vertical component (the 1D correction is only applied to the horizontal components, and thus the red and green curves coincide in the vertical component). A positive (negative) bias depicts overprediction (underprediction). The solid lines show the median FAS bias over all 259 stations, shading depicts the 95% confidence interval (CI) and the dashed lines denote one standard deviation centered at the median.

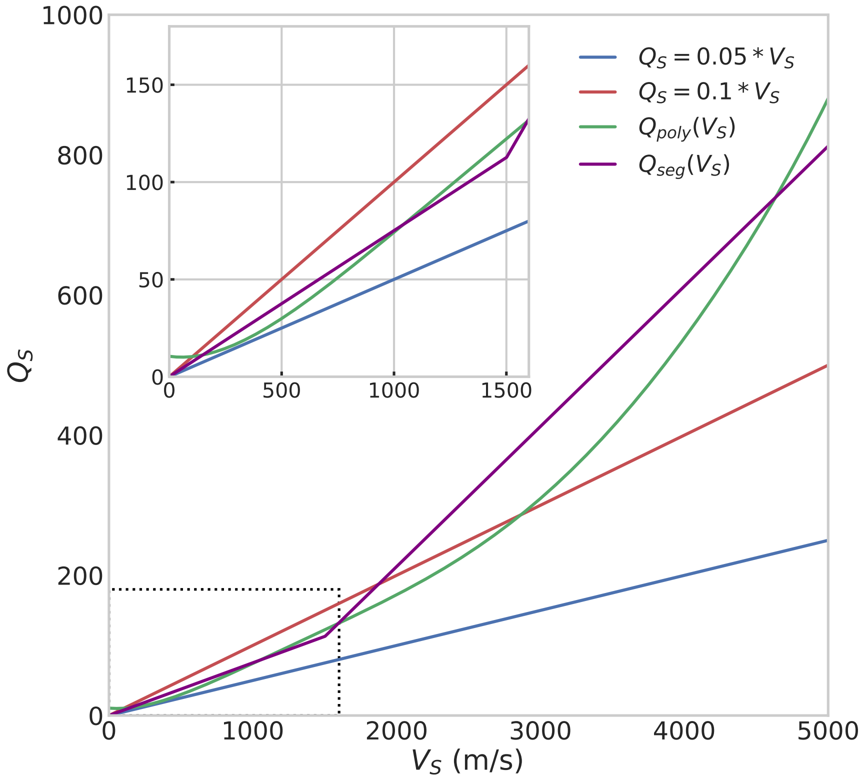

Figure S1: Shear-wave quality factor (Q_S) plotted against V_S (m/s) for several attenuation models widely used in the literature (e.g., Olsen *et al.*, 2003; Taborda and Bielak, 2014; Savran and Olsen, 2019; Withers *et al.*, 2019) and investigated here. The inset figure in the upper left corner zooms into $V_S <= 1600$ m/s, denoted by the dashed black box. Note that these Q_S relations are valid for constant Q models, or frequency-dependent Q models for frequencies below 1 Hz.

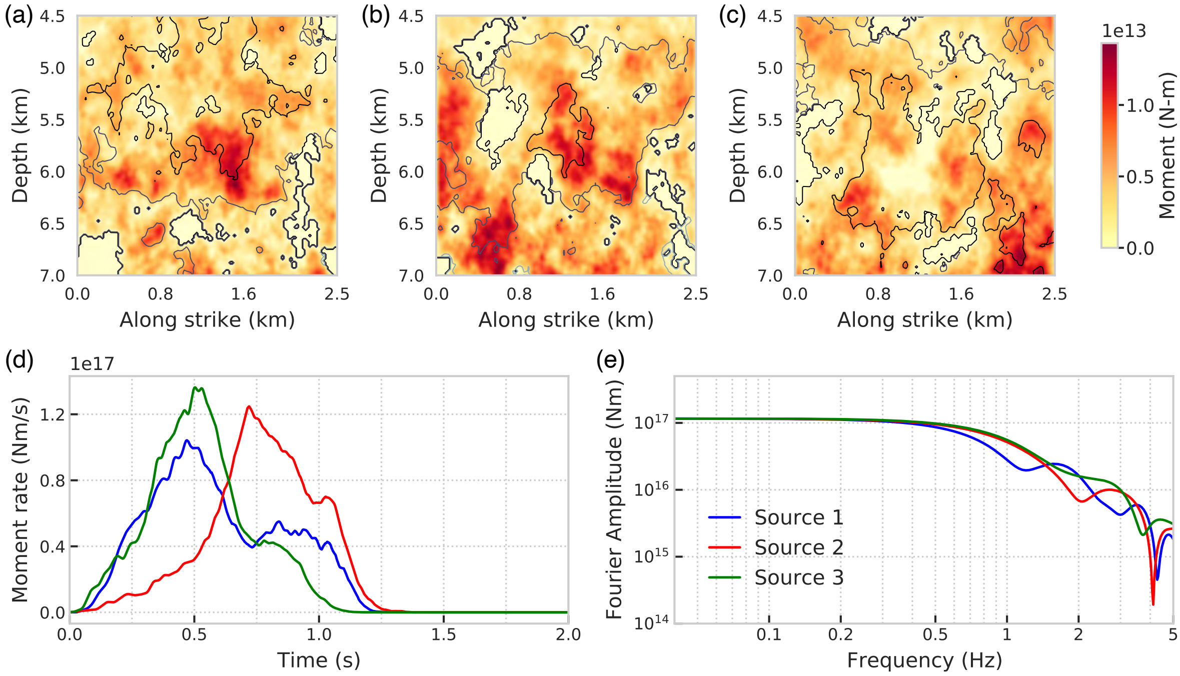

Figure S2: Description of three candidate source models used in this study. (top) Slip distribution (shading) for sources 1, 2 and 3 (a-c), characterized by their hypocentral depths of 5, 5.5 and 6 km, respectively. Contours depict rupture times at 0.4 s interval starting from 0. (d) sum of the moment rates for all subfaults and (e) Fourier amplitude spectra. Source 1 is the default source model used elsewhere in this paper.

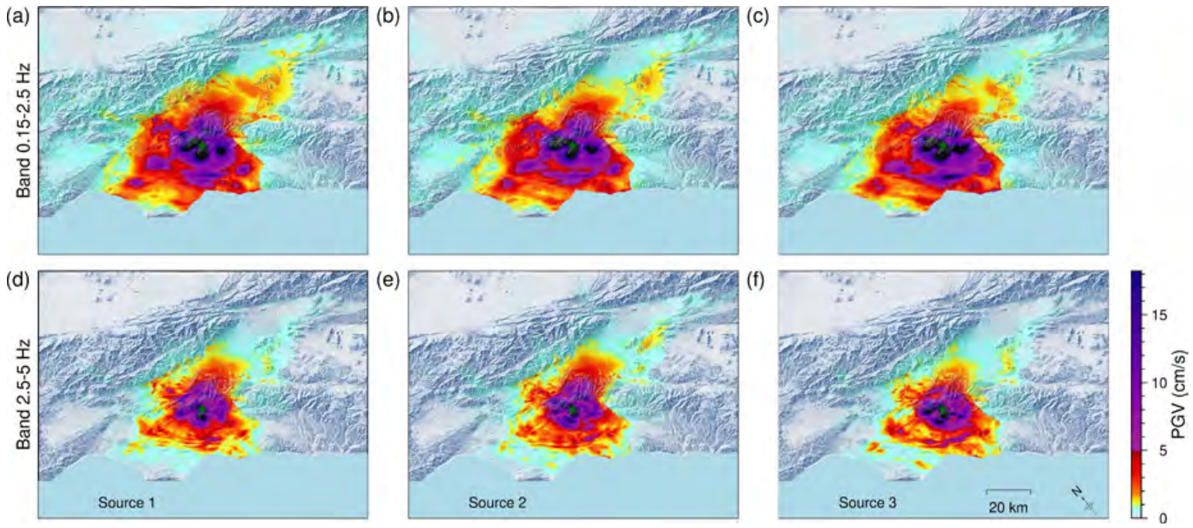

Figure S3: PGVs for sources 1, 2 and 3 (from left to right; see Fig. S2). The top and bottom rows represent the band-pass filtered results for 0.15-2.5 Hz and 2.5-5 Hz, respectively. The star denotes the epicenter of the La Habra event.

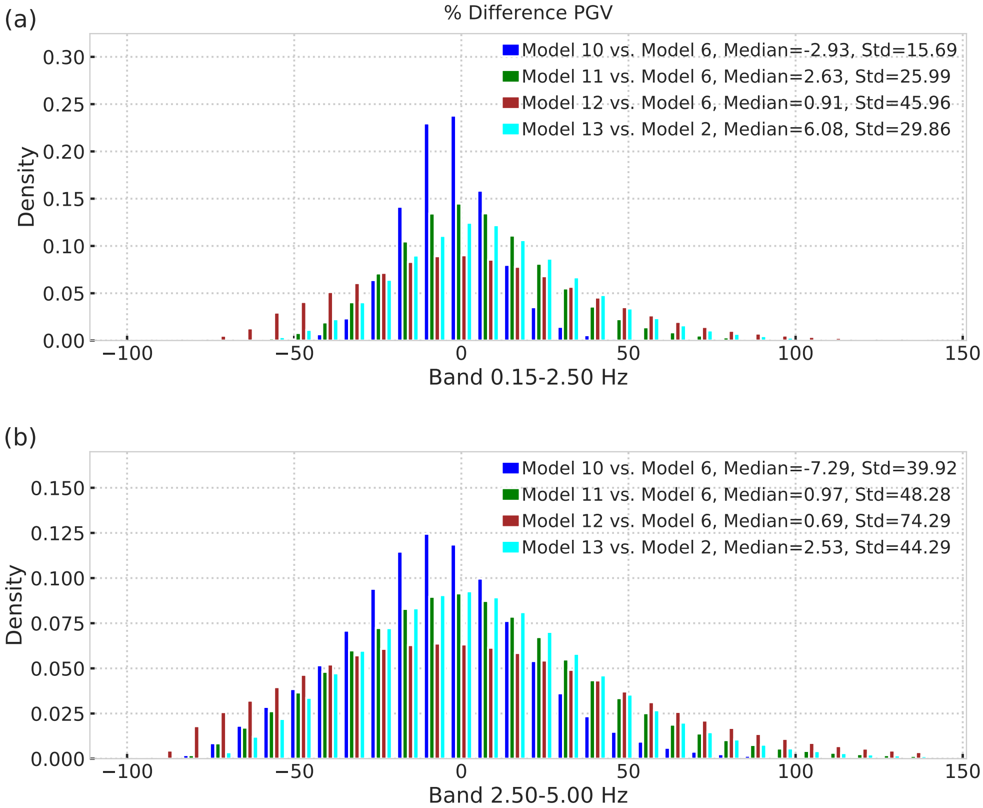

Figure S4: Effect of SSHs on PGVs illustrated by probability density histograms of the PGV difference between models with (Models 10, 11, 12 and 13) and without (Models 2 and 6) SSHs. The definition of percent difference (x-axis) is the same as in Fig. 11.

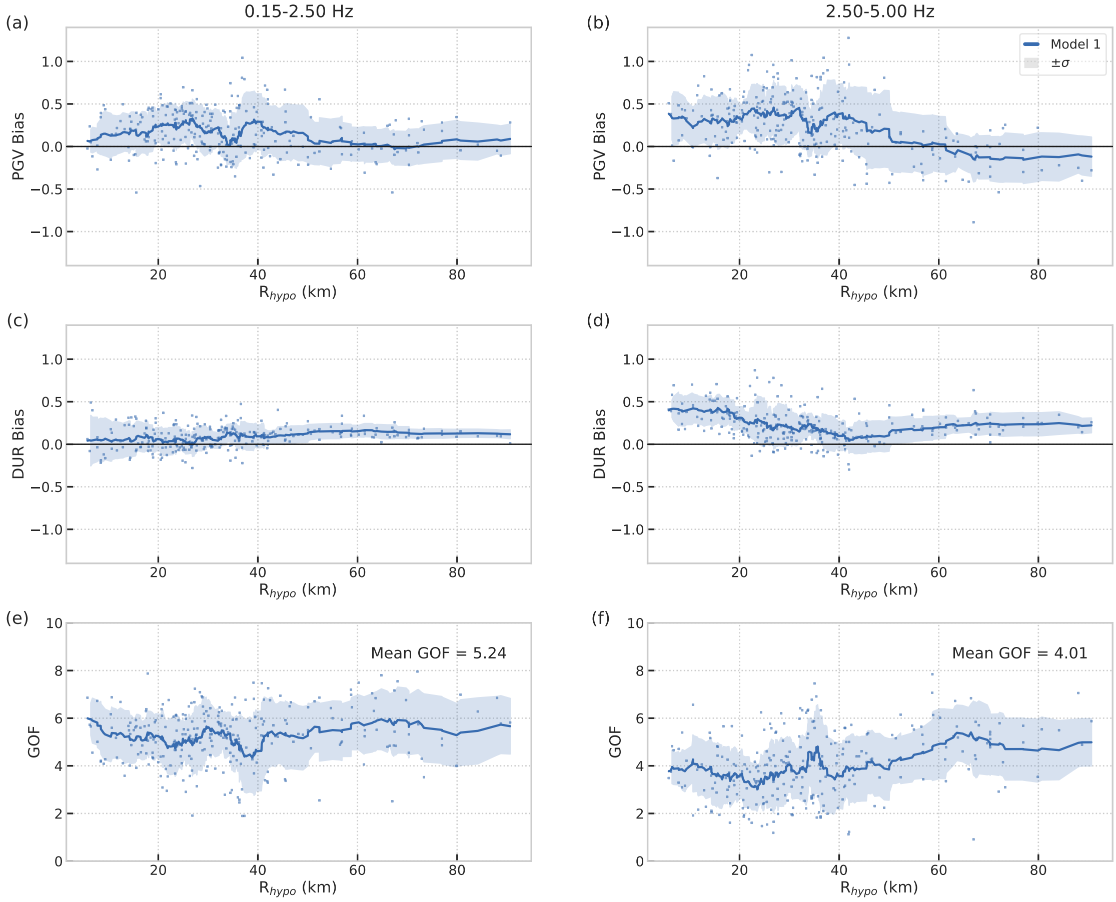

Figure S5: Bias of (top row) PGV and (middle row) DUR and (bottom row) GOF for bandwidths of (left column) 0.15-2.5 Hz and (right column) 2.5-5 Hz at all 259 stations for Model 1 (see Table 2 for model features). The bias is calculated in the same way as in Fig. 9. The solid line depicts the moving average of the bias of PGV using a 20-point window versus hypocentral distance. The shading denotes the standard deviation centered at the mean.

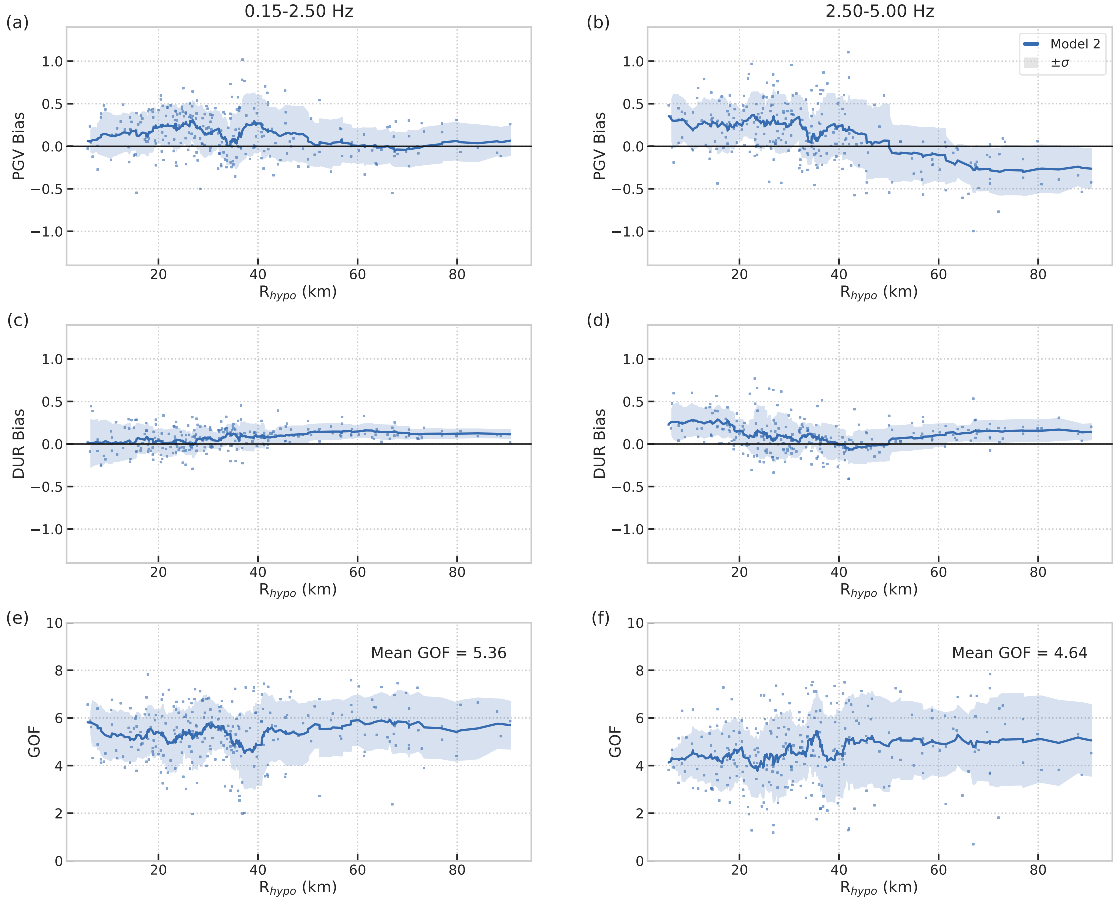

Figure S6: Same as Fig. S5, but for Model 2.

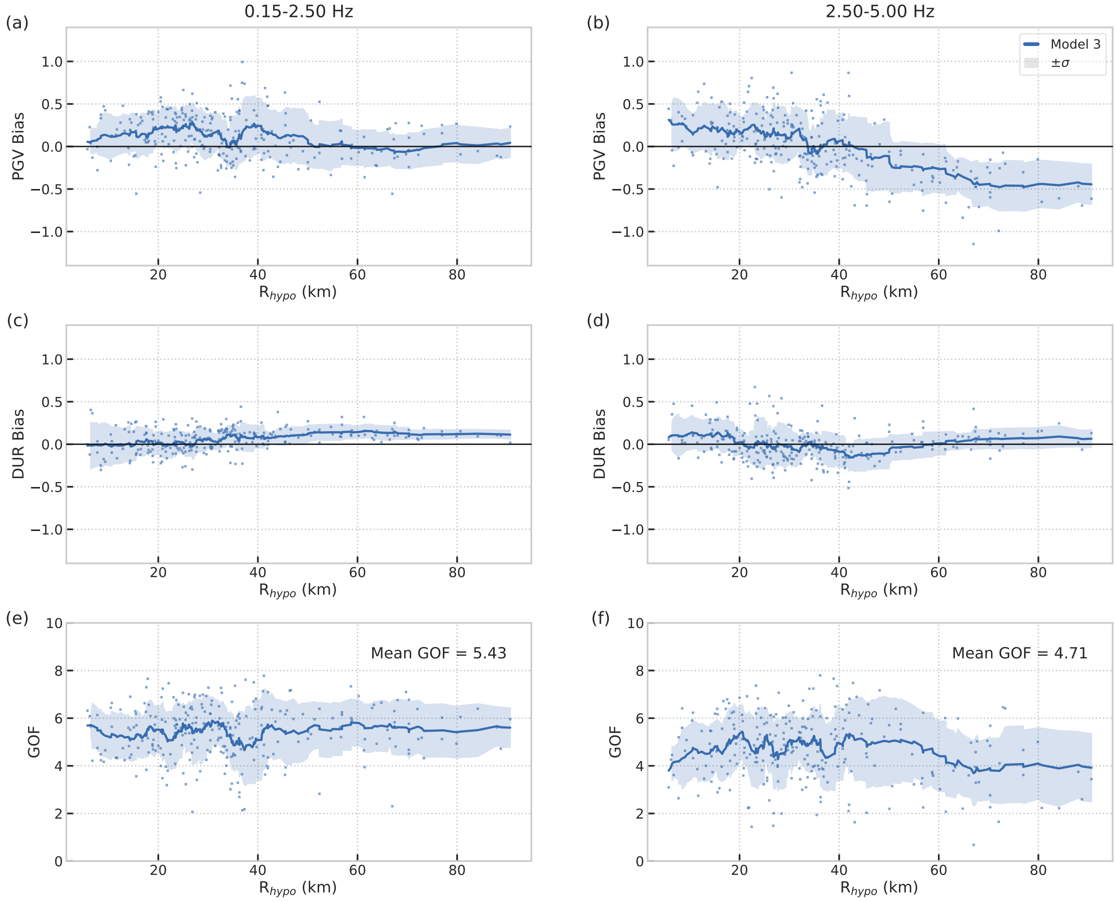

Figure S7: Same as Fig. S5, but for Model 3.

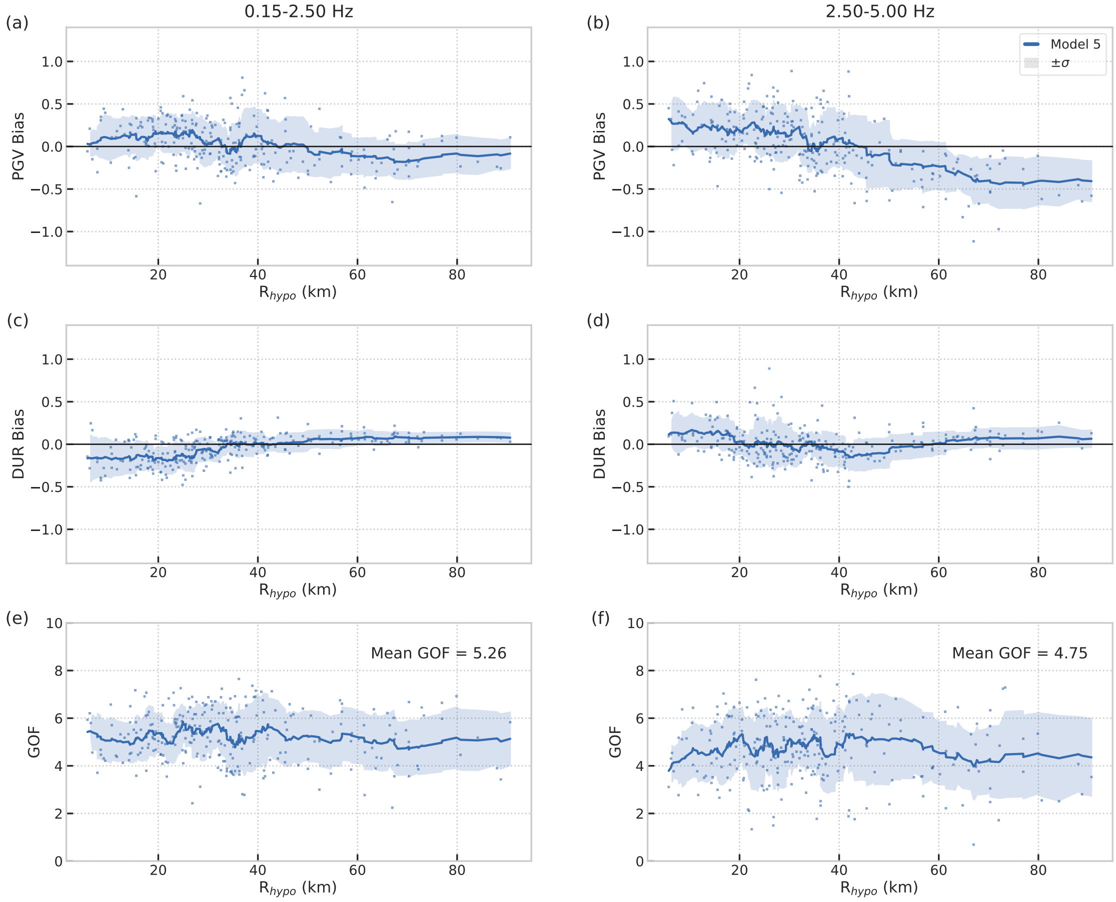

Figure S8: Same as Fig. S5, but for Model 5.

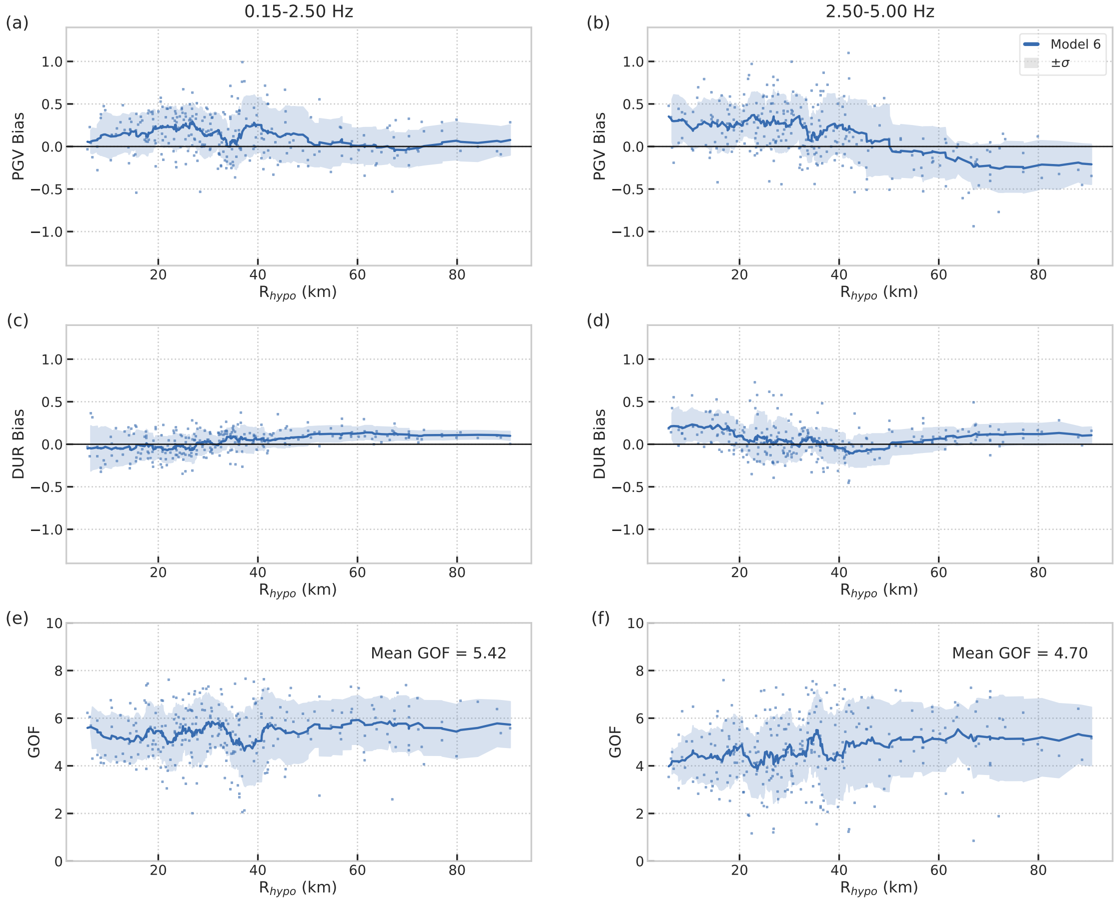

Figure S9: Same as Fig. S5, but for Model 6.

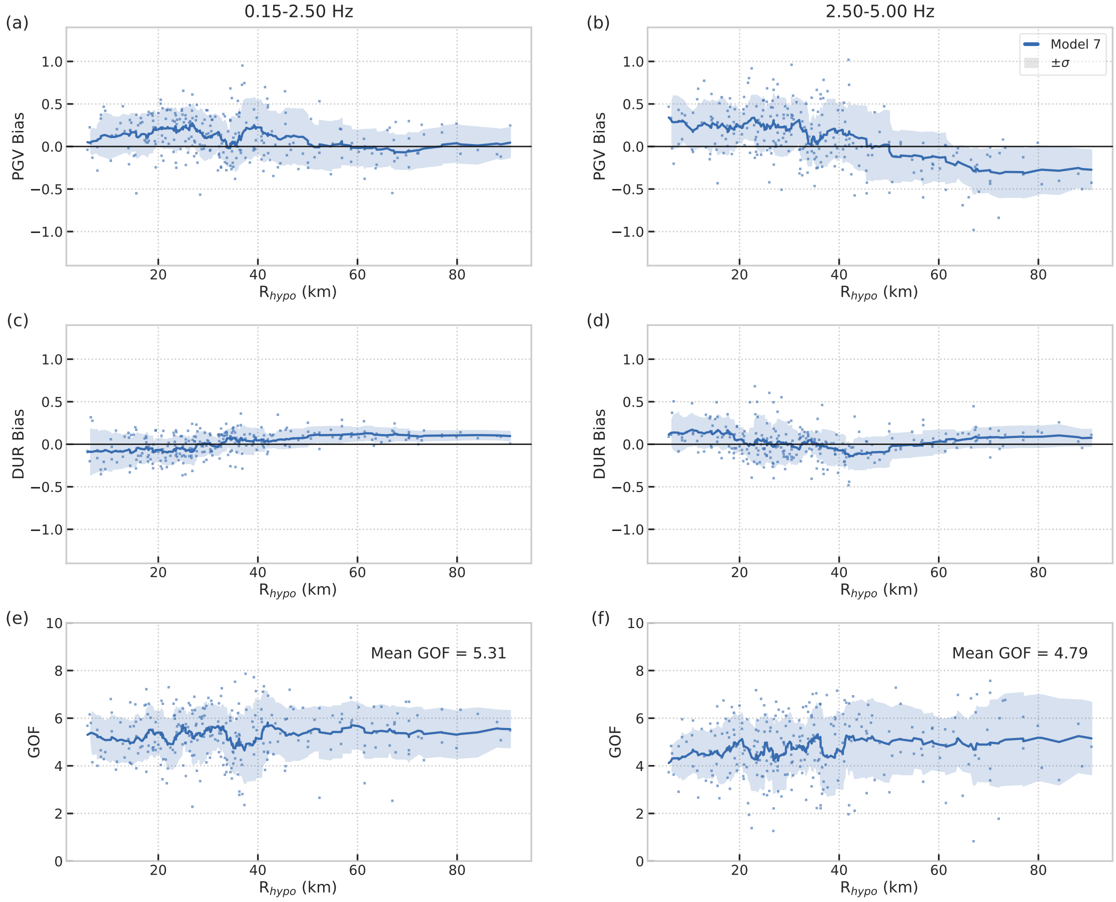

Figure S10: Same as Fig. S5, but for Model 7.

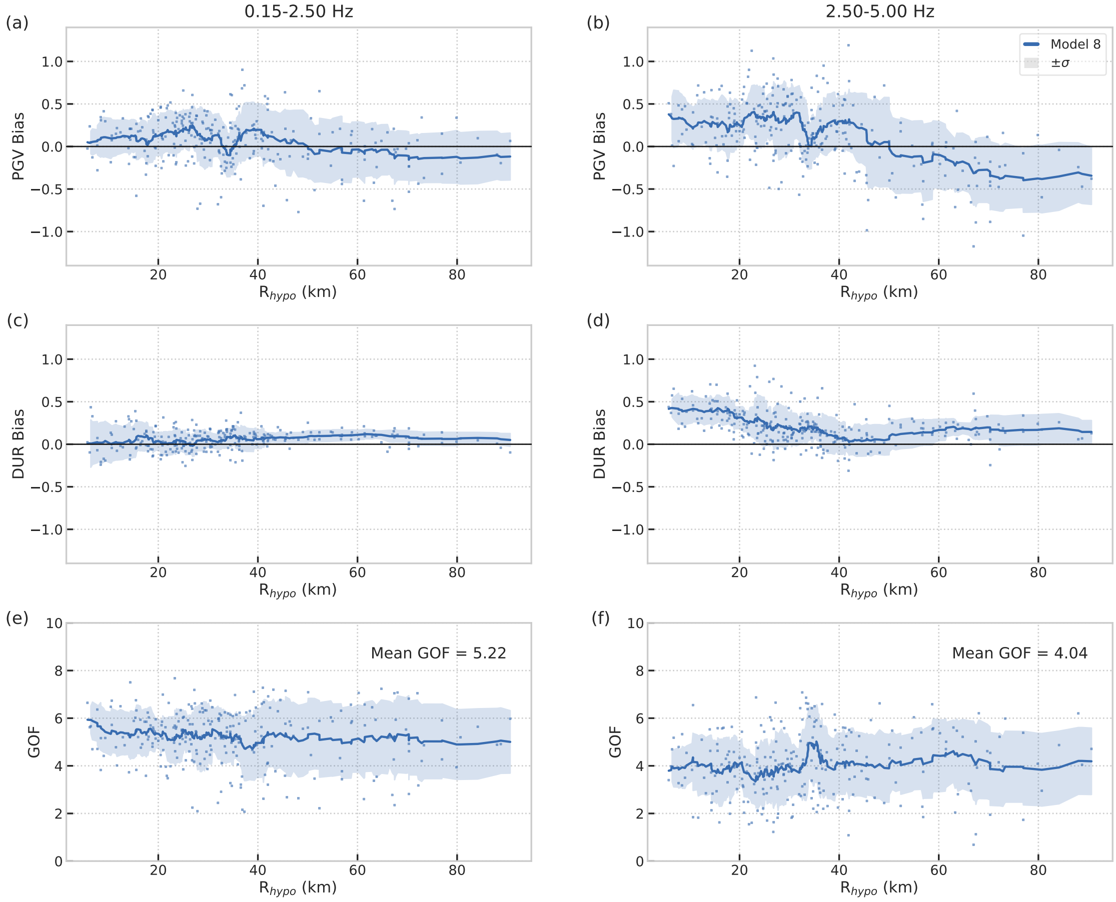

Figure S11: Same as Fig. S5, but for Model 8.

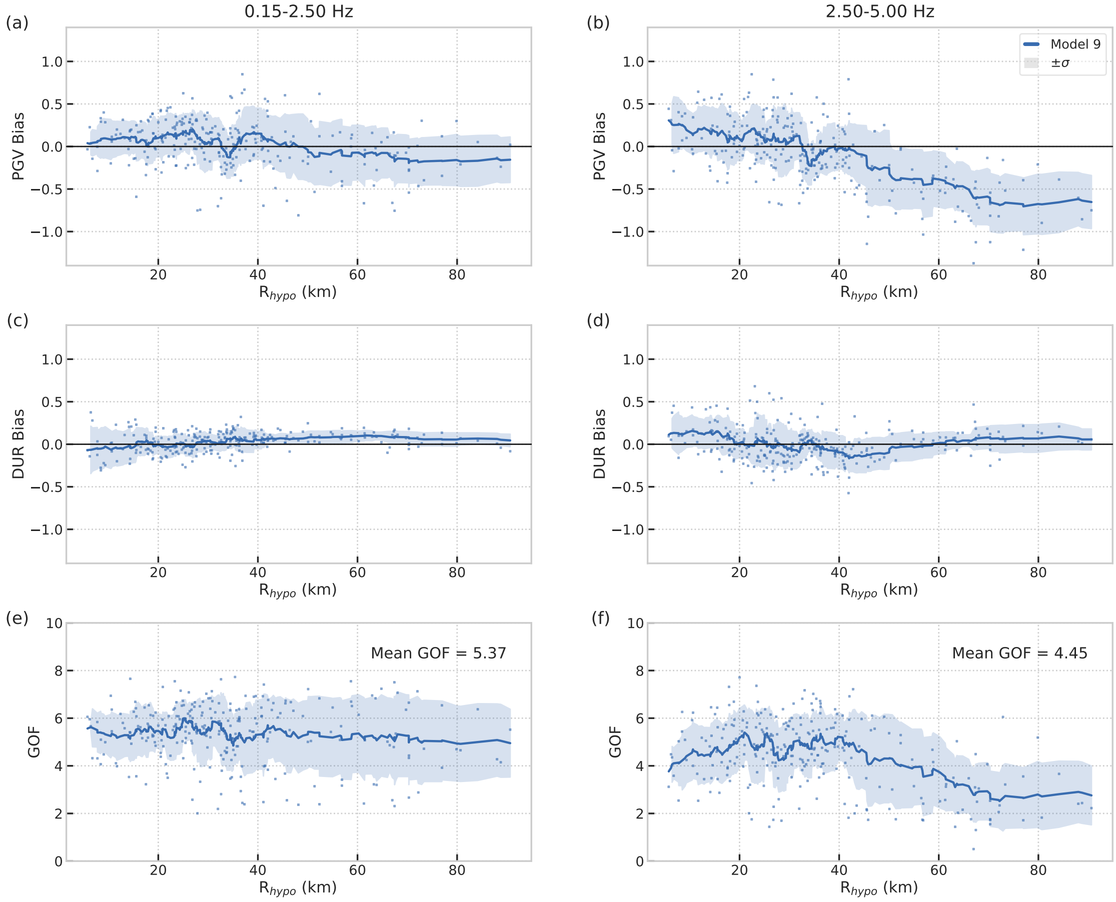

Figure S12: Same as Fig. S5, but for Model 9.

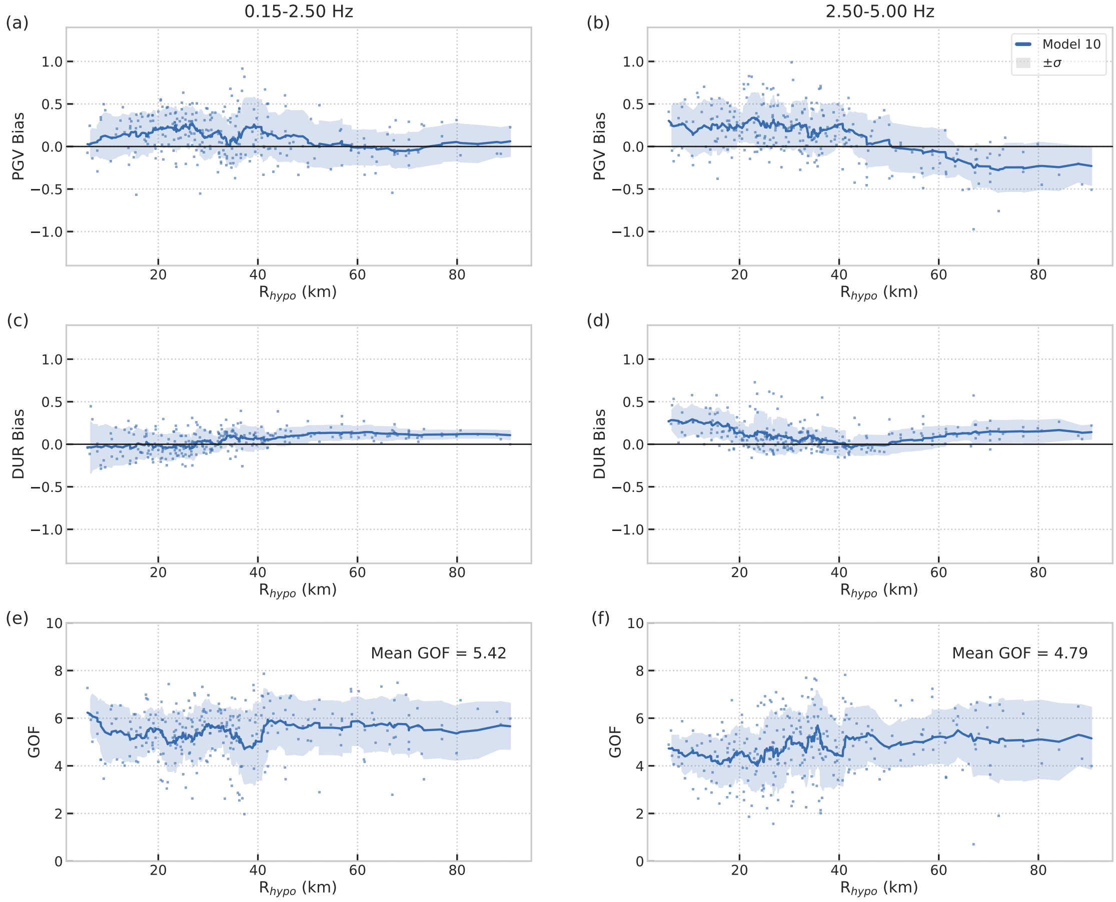

Figure S13: Same as Fig. S5, but for Model 10.

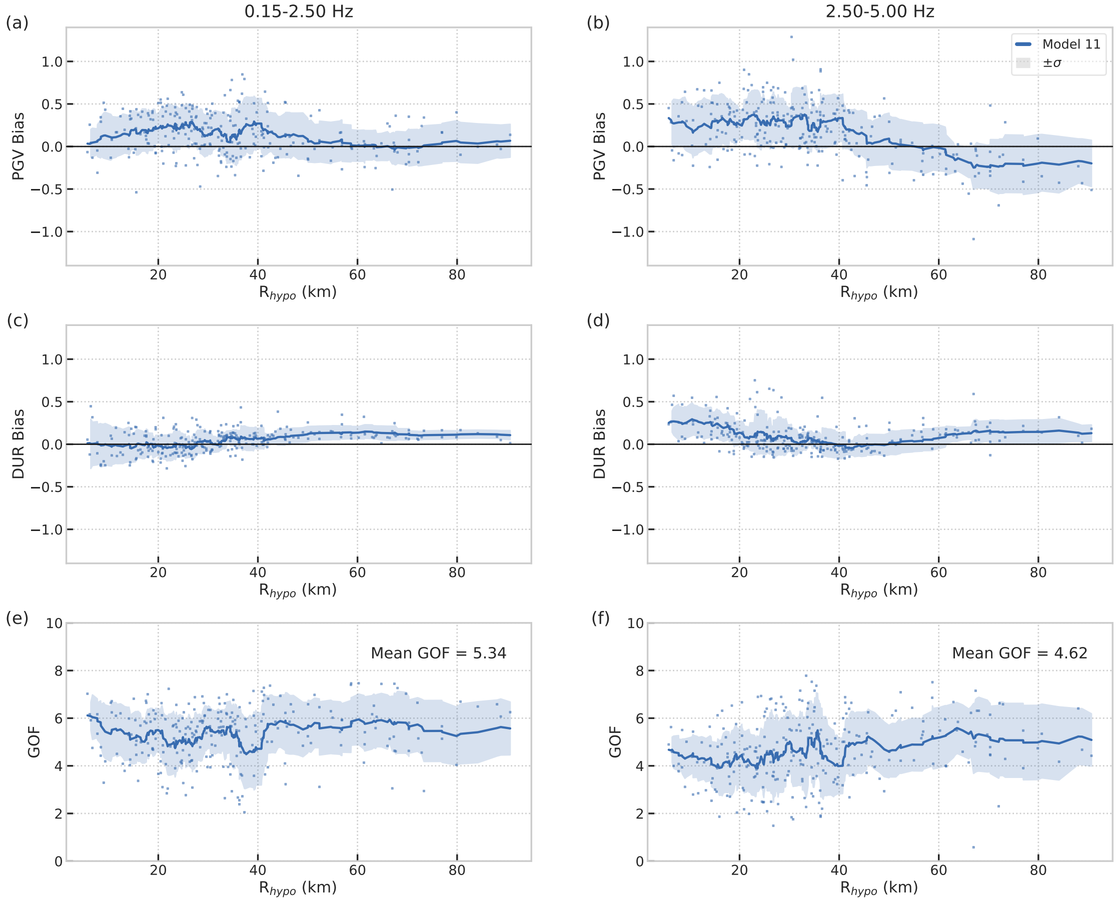

Figure S14: Same as Fig. S5, but for Model 11.

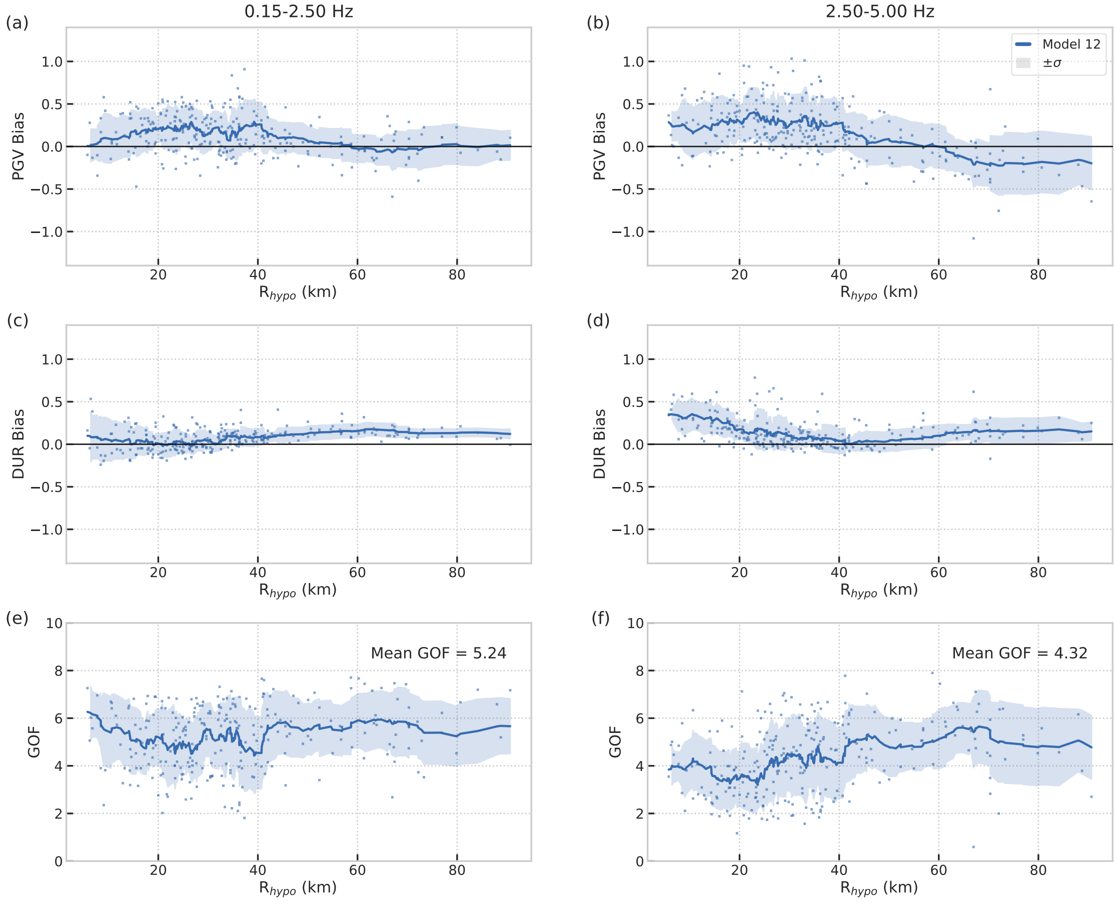

Figure S15: Same as Fig. S5, but for Model 12.

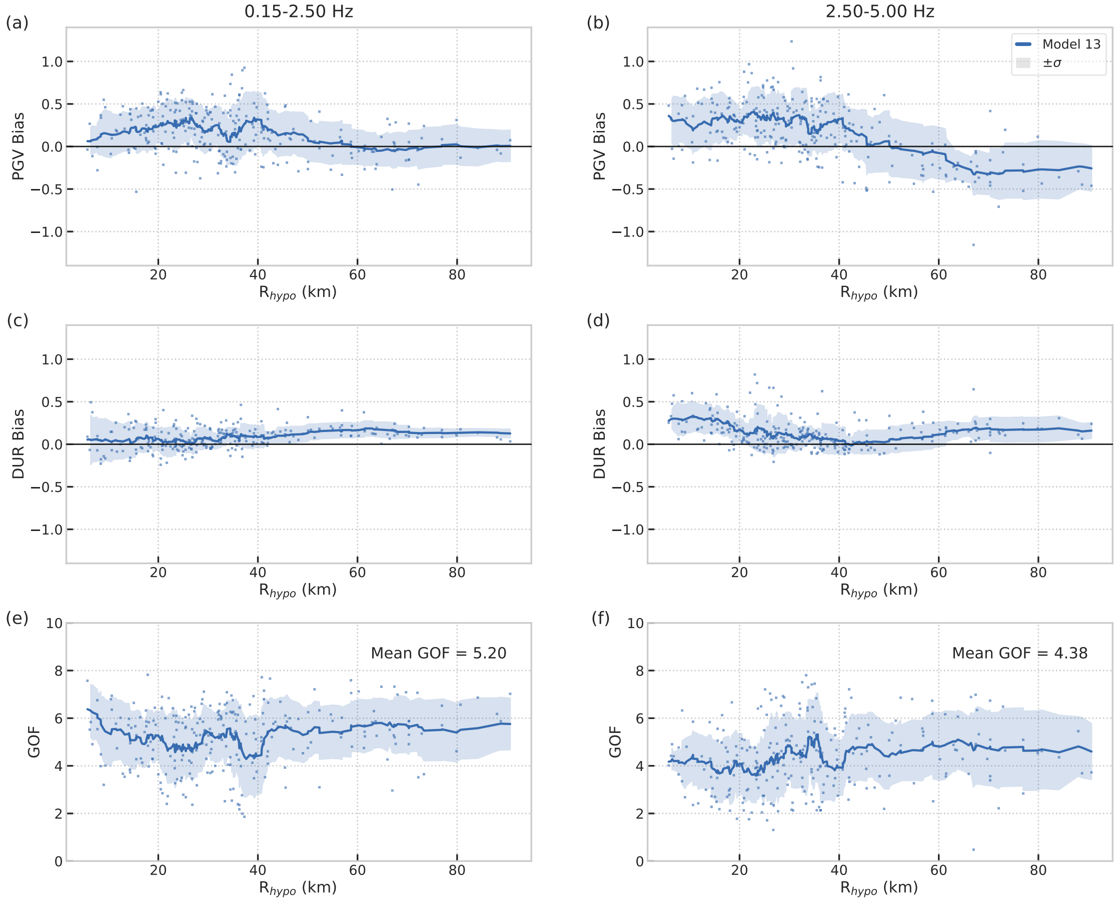

Figure S16: Same as Fig. S5, but for Model 13.

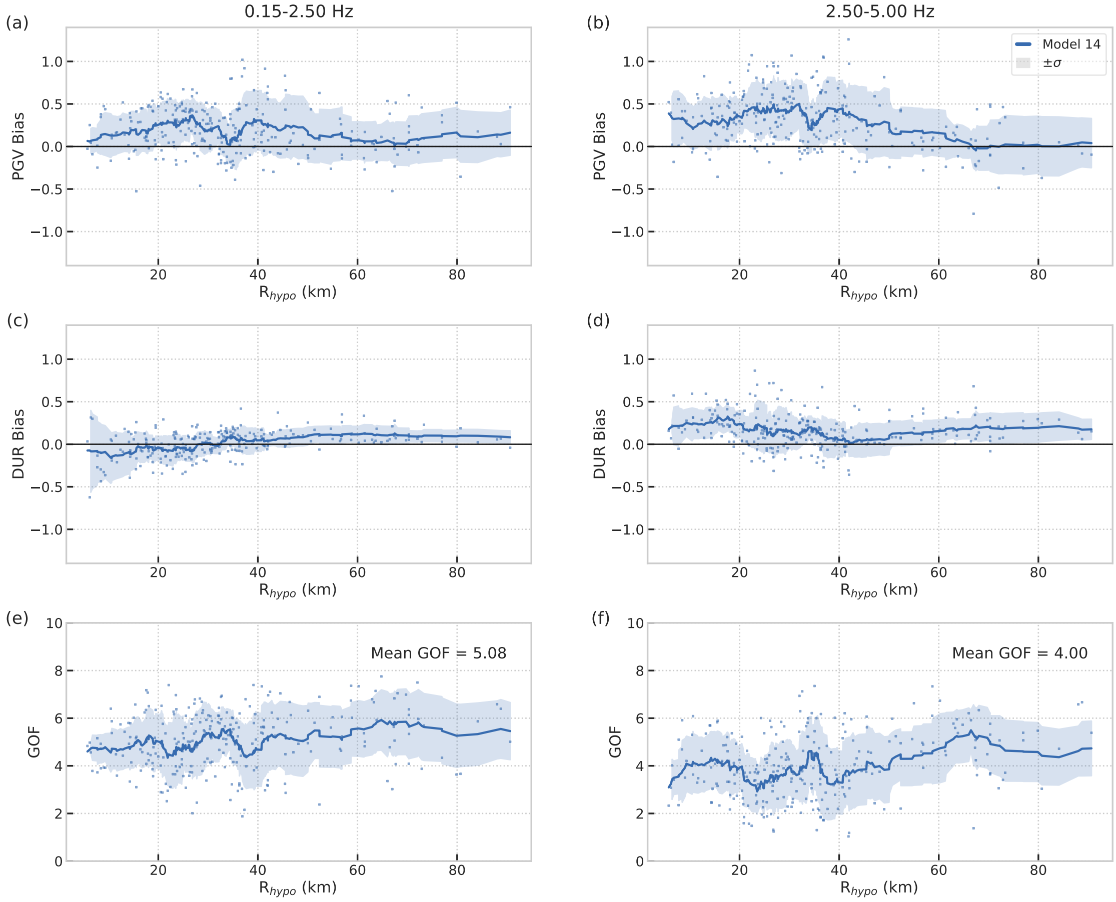

Figure S17: Same as Fig. S5, but for Model 14.

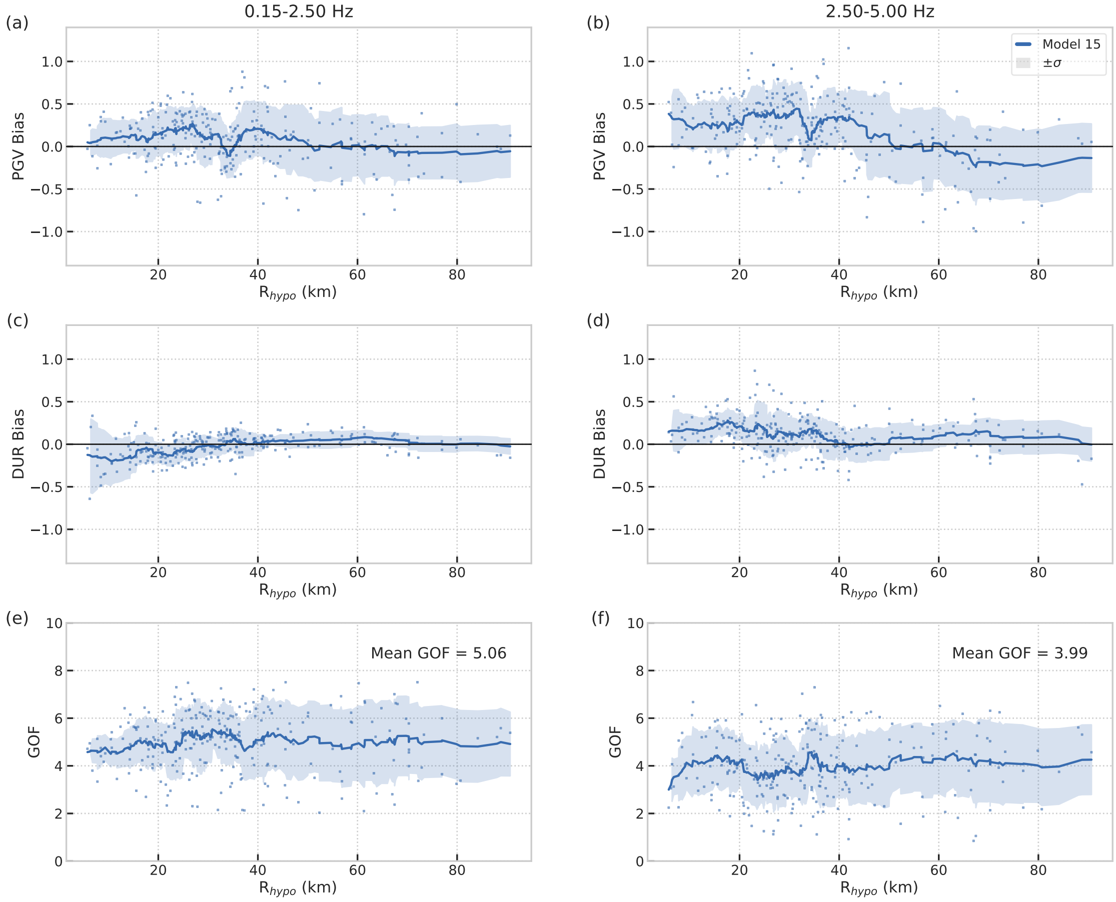

Figure S18: Same as Fig. S5, but for Model 15.

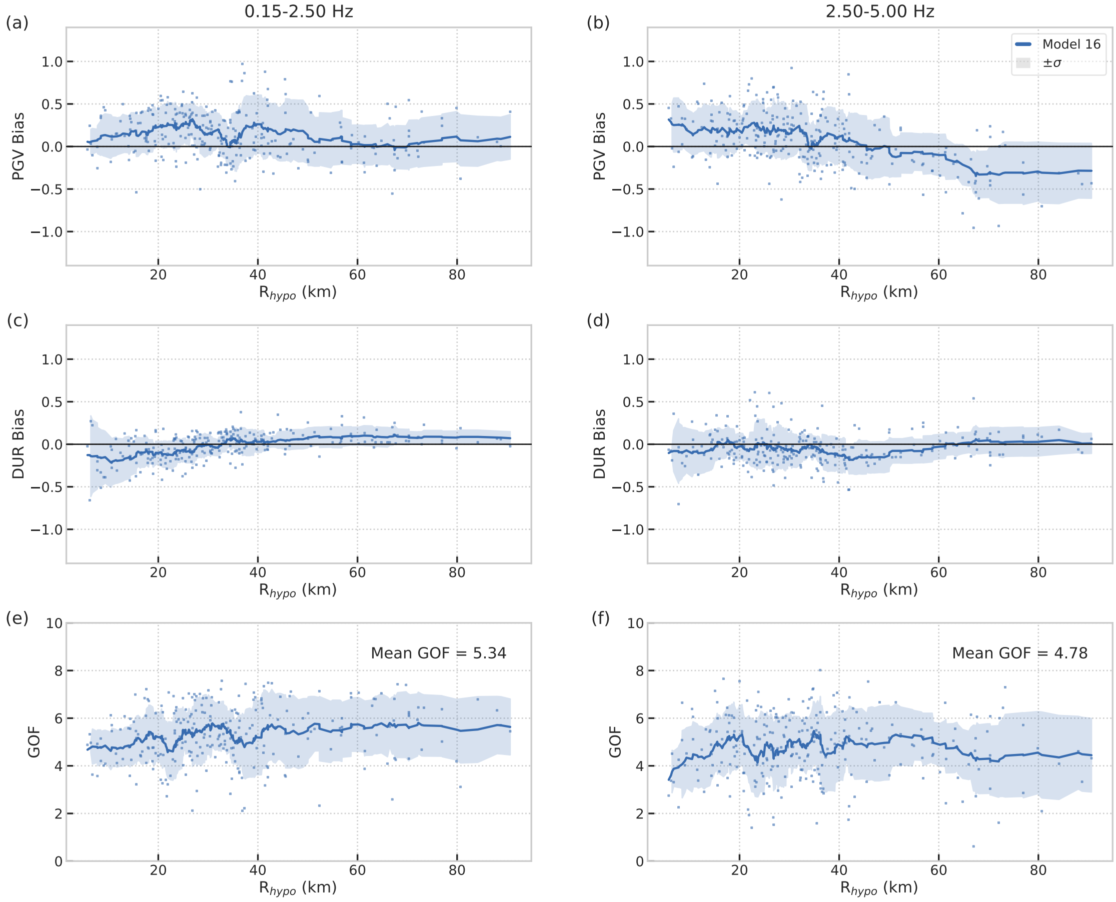

Figure S19: Same as Fig. S5, but for Model 16.

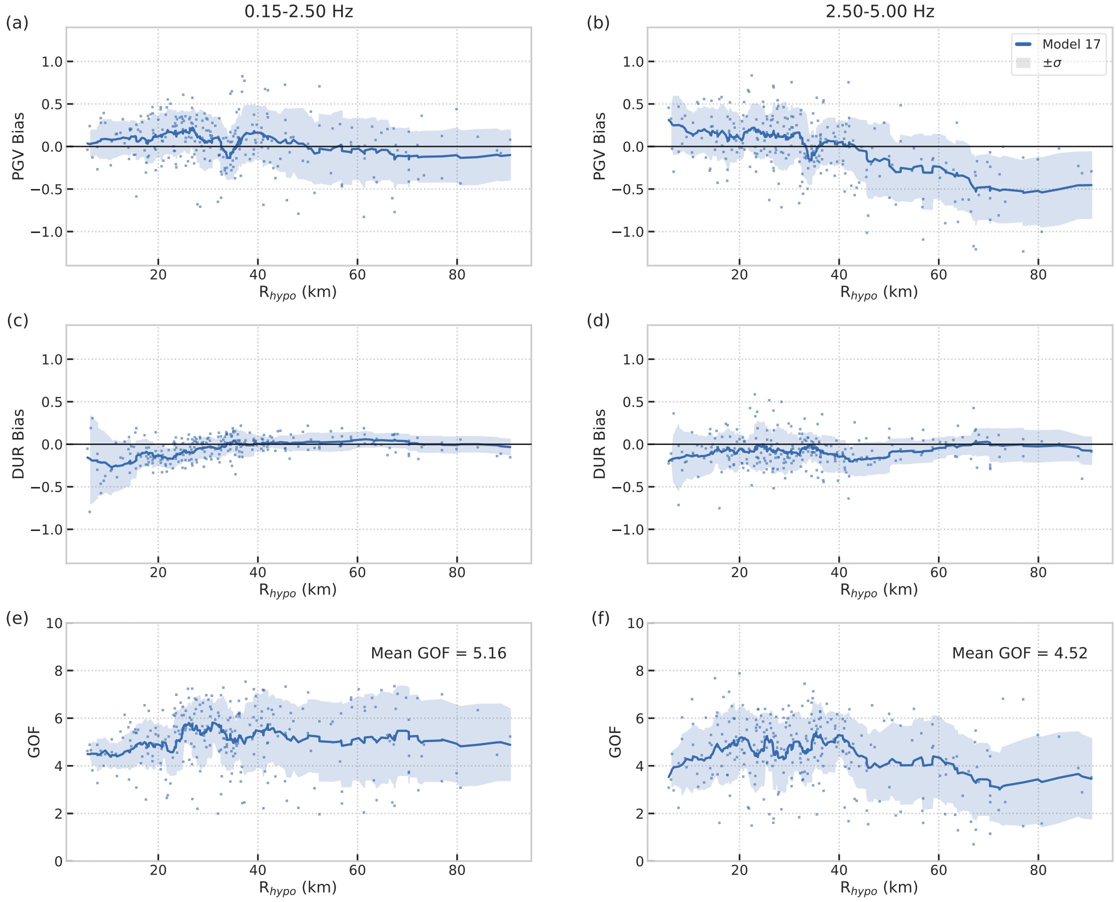

Figure S20: Same as Fig. S5, but for Model 17.